arXiv:astro-ph/0103311v1 20 Mar 2001

Circumstellar structure of RU Lupi down to au scales

M. Takami[1], J. Bailey[2], T.M. Gledhill[1], A. Chrysostomou[1] and J.H. Hough[1]

[1]Department of Physical Sciences, University of Hertfordshire, Hatfield, Herts AL10 9AB, UK.

[2]Anglo-Australian Observatory, PO Box 296, Epping, NSW 1710, Australia

Accepted by MNRAS

Abstract

We have used the technique of spectro-astrometry to study the milli-arcsecond scale structure of the emission lines in the T Tauri star RU Lupi. The wings of the Hα emission are found to be displaced from the star towards the south-west (blue wing) and north-east (red wing) with angular scales of 20-30 milli-arcsecs. This structure is consistent with a bipolar outflow from the star. From a study of the variability of the intensity and position spectra we argue that a combination of magnetically-driven bipolar outflow and accreting gas contribute to the Hα emission. On the other hand, the [OI] and [SII] emission are displaced from the star to the south-west but at much larger distances than the Hα, hundreds of milli-arcsecs for the high-velocity component (HVC) and down to 30 milli-arcsecs for the low-velocity components (LVC). The presence of both red-shifted and blue-shifted outflows in Hα but only a blue-shifted outflow in the forbidden lines can be explained if the disc obscures the red-shifted forbidden line outflow, but a disc gap with outer radius 3-4 au allows the red-shifted Hα to be seen. This gap could be induced by an unseen companion.

1 Introduction

Optical emission lines from pre-main-sequence stars are observed as clues to understanding the acceleration of jets and mass accretion on to the stars. The spatial resolution of most techniques is insufficient to resolve their dynamics directly, while high-resolution spectroscopy has provided a variety of information for these mechanisms. Hα emission shows a rich variety of profiles due to an interplay between emission and absorption features (e.g., Reipurth, Pedrosa, & Lago 1996), and various models have been discussed to explain their profiles using accelerating stellar wind (e.g., Decampli 1981), decelerating stellar wind (Mitskevich, Natta, & Grinin 1993), disc wind (Calvet, Hartmann, & Hewett 1992), and infalling envelope (e.g., Calvet & Hartmann 1992). The forbidden lines often have two blue-shifted velocity components, which have provided constraints on geometry and mechanism of jet and/or wind (Eislöffel et al. 2000, and references therein). The lack of red-shifted components of these line supports the existence of circumstellar discs (Eislöffel et al. 2000, and references therein). In addition to high-resolution spectroscopy, some techniques have been tried in the last decade to obtain spatial information. Speckle observations reveal elongated structure of the Hα emission with an angular scale of 0.09 arcsec towards T Tau (Devaney et al. 1995). The *Hubble Space Telescope* has provided fine structure of jets towards young stellar objects (Ray et al. 1996; Burrows et al. 1996) although the bandwidths of its filters are often insufficient to suppress the stellar continuum from pre-main-sequence stars. Ground-based long-slit spectroscopy is effective in measuring the typical angular scale of a few forbidden lines suppressing the contamination of the strong continuum emission (e.g., Hirth, Mundt, and Solf 1997).

Here we present the results of spectro-astrometric observations of RU Lupi. The spectro-astrometry technique studies the small scale structure by observing the relative position of the centroid of the point-spread function on scales of a few milli-arcsec (Bailey 1998a, b). The target, RU Lupi, is one of the most active T-Tauri stars in the southern sky. The Hα emission has broad wings up to 900 km s^{-1} (Reipurth, Pedrosa, & Lago 1996), and the equivalent width of the emission line is up to 200 Å, which is one of the largest among T-Tauri star (Giovannelli et al. 1995). Forbidden lines of [SII] and [OI] are also present in the spectrum of RU Lupi, and at least the [OI] lines have an extended blue wing up to 300 km s^{-1} and a redder peak up to 30 km s^{-1} (Gahm, Lago, & Penston 1981; Hamann & Persson 1992). In this paper, the detail of the observations and the data reduction are described in §2, the results are shown in §3, and the origin of Hα emission and the forbidden lines are discussed in §4 together with the existence of a circumstellar disc with a gap. Throughout this paper, the distance of 140 pc to the Lupus cloud is adopted based on Hughes, Hartigan, & Clampitt (1993).

2 Observations & Data Reduction

Observations were carried out on 1996 Aug 25, 1997 Jun 27, and 1999 Jul 2 at the 3.9-m Anglo-Australian Telescope using the RGO spectrograph. The configuration with a 1-arcsec slit width, a 1200 line mm^{-1} grating, and the 82-cm camera provided a spectral resolution ($\lambda/\Delta\lambda$) of 7000. The first two observations used a Tektronix 1024×1024 thinned CCD. The 1999 Jul 2 observation used a 2048×4096 deep depletion CCD from MIT Lincoln Labs. The pixel scale was 0.23 arcsec with the Tektronix CCD and 0.15 arcsec with the MITLL CCD, which provides good sampling of the seeing profile (1–1.5 arcsec) at each wavelength. The spectra were obtained at four slit position angles (0°, 90°, 180°, and 270°). The flat fields were made by combining many exposures with the spectrograph illuminated by a tungsten lamp. Wavelength calibrations were made by observations of a CuAr lamp.

The data were reduced using the FIGARO package. After subtracting the bias level and flat-fielding, the position spectrum was determined by fitting the seeing profile at each wavelength with a Gaussian function. About 1-2×10^4 photons at each wavelength provides a typical accuracy of 2-5 milli-arcsec at the continuum level. Any instrumental effect in the position spectra were eliminated with high accuracy by subtracting those with opposite position angles ($0\,^\circ - 180^\circ$, or $90\,^\circ - 270^\circ$), since these will remain constant on rotation whereas any real structure in the source will reverse its sign. Effects which are removed in this way include any curvature or optical distortion introduced by the spectrograph, any misalignment of the spectrum with the CCD columns, and any effects due to departure of the CCD pixels from a regular grid, imperfect flat fielding, or charge transfer deficiencies in the CCD. The derived position spectra have wavelength coverages of 6520-6750 Å for the former two runs and 6160-6780 A for the latest run, which include Hα, [SII] 6716/6731 A, [NII] 6583 A, and [OI] 6300 Å. Each position spectrum has an arbitrary zero point, which we adjust to correspond to the continuum position. In addition to the position spectra, the intensity spectra were obtained by subtracting the bias, flatfielding, subtracting the adjacent sky and extracting bright columns on the CCD. In all the spectra, the radial motion of the star is calibrated using the Li 6707.815Å absorption line on the stellar atmosphere. The measured radial velocity in the local standard rest frame is $+8 \pm 2$ km s^{-1}.

Similar methods were previously used by Hirth, Mundt, and Solf (1994, 1997) to study forbidden emission lines in pre-main sequence stars. However, the techniques described here enable us to achieve substantially higher accuracy in the relative positions.

3 Results

3.1 Positional displacement and intensity profile of Hα, [OI] and [SII] emission

Fig. 1 shows the raw spectra of the intensity and the positional displacement. In the intensity spectra, a number of emission lines including Hα, HeI, [SII], [OI], [NII], FeI, FeII, and SiII are detected. The wavelengths and equivalent widths without atmospheric correction are summarized in Table 1.

Among these lines, the Hα, [SII] 6731/6716Å, [NII] 6583 Å, and [OI] 6300 Å lines show displacements from the continuum position in the position spectra. The positions shown in Fig. 1 are the centroid of the combined line and continuum emission of the star, that is, the centroid of their positions weighted by their intensities. To get the true position of the emission line region the observed position must be corrected for the effect of the underlying continuum by dividing the positional displacement in the raw spectra by $I_{\lambda(\mathrm{line})}/(I_{\lambda(\mathrm{line})} + I_{\lambda(\mathrm{conn})})$. Fig. 2 shows the positional displacement of Hα, [OI] 6300 Å, and [SII] 6731/6716 Å observed on 1999 Jul 2 after this calibration. Typical uncertainties for the displacements in Fig. 2 are 2, 15, 40, and 100 milli-arcseconds for Hα, [OI] 6300 Å, [SII] 6731 Å and 6716 Å, respectively. For Hα, higher accuracy was obtained than that at the continuum level because of its brightness while the accuracy of the other forbidden lines are much less than the continuum because of their lower intensity. The line profiles shown in Fig. 2 are similar to those previously presented by Giovannelli et al. (1995), Reipurth, Pedrosa, & Lago (1996), and Hamann (1994).

Fig. 2 shows that the positional displacement of Hα emission extends towards the south-west and the north-east over angular scales of up to 20-30 milli-arcsec. The intensity profile of Hα emission is symmetric except for a redshifted absorption dip at +50 km s^{-1} from the star, and the blue-shifted wing corresponds to the displacement at the south-west while the red-shifted wing corresponds to that at the north-east. At these wings, the displacement monotonically increases with the relative velocity from the star in the velocity ranges of -50 to -200 km s^{-1} and +200 to +300 km s^{-1}. On the other hand, the displacement is distributed within 5 milli-arcsec from the star in a lower velocity range between -50 and +200 km s^{-1}, and does not show clear correlation with the velocity in Fig. 2.

The positional displacement of the three forbidden lines extends only towards the southwest, the same direction as those of the blueshifted Hα wing, and that of HH55 which lies 3 arcmin from RU Lupi (cf. Krautter, Reipurth, & Eichendorf 1984). The displacements are larger than that of Hα emission by a factor of 10-30, and smallest in [OI] and largest in [SII] 6716Å: up to 200, 400, and 600 milli-arcsecs for [OI] 6300Å, [SII] 6731 Å, and 6716Å, respectively. These line profiles show two peaks with typical velocities between -250 and -100 km s^{-1} for the high velocity component (HVC) between -100 and 0 km s^{-1} for the low velocity component (LVC). The HVC is more extended spatially than in the LVC as in other T Tauri stars. The typical angular scales of the LVC are 30-40 milli-arcsec in [OI] 6300 Å and 150 milli-arcsecs in [SII] 6731 Å. Fig. 2 does not show a clear difference in the displacement between the two components in [SII] 6716Å.

The relation between the velocity and the radial distance of the displacement for Hα, [OI] 6300Å, and [SII] 6731Å, is plotted in Fig. 3. A higher signal to noise ratio of the positional displacements has been obtained by binning along the wavelength. This figure shows that the velocity monotonically increases with the distance for all the lines, and the gradient for Hα emission is much larger than those for the forbidden lines. Fig. 3 also shows slight asymmetry of the velocity field between the blueshifted and red-shifted wings of Hα emission: the positional displacement is prominent in the figure beyond the velocity of 100 km s^{-1} for the blue-shifted wing and 200 km s^{-1} for the redshifted wing. In the forbidden lines, the displayed velocity gradient is larger in the HVC (ΔV $>$ 100 km s^{-1}) and smaller in the LVC (ΔV$<$100 km s^{-1}). On the other hand, the LVC in [OI] reveals no velocity gradient while those in the [SII] 6731 Å line show slight positive gradients. The position of the LVC is offset from the star even at the zero velocity: 30 and 70 milli-arcsecs for [OI] and [SII] 6731 Å, respectively.

The observed tendencies for the line profiles and the positional displacement of the HVC agree with the previous observations of other T Tauri stars. Ground-based long slit spectroscopy shows the positional displacement of the HVCs of T Tauri stars in the Taurus-Auriga cloud (Hirth, Mundt, and Solf 1997), which lies at a similar distance (140 pc) to that of the Lupus cloud. The HVC and LVC in these objects have typical velocities -50 to -150 km s^{-1} and -5 to -20 km s^{-1}, respectively, which are similar to those of RU Lupi. The measured displacements of the HVC are 0.2 and 0.6 arcsecs for [OI] and [SII] 6731Å, respectively, which are similar to those seen in our observations. The [SII] lines have much lower critical density than the [OI] line (typically 10^3 and 10^6 cm^{-3}, respectively), and the observed positional difference between these lines indicates that the outer region has a lower electron density. Such a distribution of the electron density could be due to diverging stream lines of the outflow, as suggested by Hirth, Mundt, and Solf (1997).

3.2 Time variation of Hα and [SII] emission

Fig. 4 shows the time variation of the intensity profile and the positional displacement for Hα, [SII] 6731Å, and [SII] 6716Å emission. Since photometric observations were not made on the same dates, each line profile is displayed in a unit of the continuum intensity on each date. The positional displacements are displayed after removal of the contamination of the continuum, as in Fig. 2.

In the case of Hα, time variation was detected for both the line profile and the position spectra. The intensity profiles observed on 1996 Aug 25 and 1997 Jun 27 are nearly the same at the wings. On the other hand, at the peak with the velocity of -100 to $+100$ km s^{-1}, the profile on the latter date has lower intensity relative to the continuum than that on the former date. On 1999 Jul 2, the relative intensity of the Hα to the continuum is slightly lower than the others except that at the absorption dip. In the same observing run, the absorption dip is shallower and relative intensity is higher at the top than those observed in the other runs. Clear change of the position spectra of Hα was observed during 1997-1999 with the velocity ranges of -200 to -100 km s^{-1} and $+100$ to $+300$ km s^{-1}. The positional displacements of these wings are larger on the latest date than in the others by a factor of 2-3. The repeatability of the measured positional displacement between -100 and $+100$ km s^{-1} confirms that the displacement is not due to slight oscillation of the tracking of the telescope, since any other pre-main sequence stars observed in 1999 do not show the same displacements as observed in this object.

The relative intensity of the [SII] lines to the continuum is smallest on the earliest date, and largest on the latest date at the whole velocity range. On the other hand, the peak velocity and the line widths of the HVC and LVC did not change throughout the observations. To determine the difference of the time variation between the HVC and LVC, we measure the equivalent widths of the HVC and LVC respectively, and these are tabulated in Table 2. For both the [SII] 6716Å and 6731Å, the LVC shows a larger increase in the equivalent width than the HVC: the difference of the relative intensities between 1996 and 1999 is 40-50 and 10-30 percent for the LVC and HVC, respectively. Table 2 also shows the equivalent width ratio of the two lines of 0.53-0.60 and 0.37-0.40 for the HVC and LVC, respectively, and these ratios indicate electron densities of 4-6$\times 10^3$ and more than 10^4-10^5 cm^{-3} assuming a electron temperature of 10^4 K (cf. Osterbrock 1989). Such a difference of the electron density between the HVC and LVC was also observed in other T Tauri stars by Hamann (1994). On the other hand, Fig 4. shows no systematic time variation in the position spectra of the two [SII] lines. The displayed variation would indicate motion of gas, although higher signal-to-noise ratio is required to comfirm the existence of the variation.

In addition to the time variation of the emission line fluxes, variation of the continuum flux can affect the intensity profiles shown in Fig. 4. Its contribution is not clear owing to the lack of photometric data. Previous observations show the time variation of the continuum which may be caused by obscuration by clumpy clouds (Gahm et al. 1974; Giovannelli et al. 1995). In addition, Table 1 shows time variation of the equivalent width for the Li absorption, which suggests variation of the veiling continuum. The intensity profiles of Hα and the two [SII] lines show different time variation, and it cannot be simply explained by variation of the continuum. The ratios of the equivalent width between the LVC and the Li absorption are nearly constant over time (1.4-1.6 and 0.5-0.6 for [SII]6731Å/Li and [SII]6716Å/Li, respectively), and suggest that the time variation of the LVC is due to the variation of the veiling continuum.

3.3 Comparison with the other lines profiles

The profiles of the other lines are plotted in Fig. 5. Most of the permitted lines including FeI, FeII, SiII have triangular profiles with peak velocities of -50 to $+50$ km s^{-1}, and full width zero intensities of less than 250 km s^{-1}. The width of these lines is much narrower than that of the Hα, and the velocity ranges of these lines do not overlap that of the Hα wings: thus, these lines are not related to the Hα wings observed in 1999. On the other hand, the profiles of [OI] 6364 Å and [NII] 6583 Å are much more similar to those of [OI] 6300 Å and the two [SII] lines than that of Hα. The profiles of [OI] 6364 Å, which shares the upper transition level with [OI] 6300 Å, is nearly the same as that of the latter line shown in Fig. 2. No clear signature of the LVC is found in the [NII] profile as in the case of other T Tauri stars (e.g., Hartigan, Edwards, and Ghandour 1995).

The HeI 6678 Å line shows different profiles from the others, and a prominent time variation was observed. In 1996 and 1997, the line had nearly the same triangular profile with a full width zero intensity of about 400 km s^{-1}. On the other hand, in 1999, the line width was reduced to be about a half without changing the peak velocity and the relative intensity to the continuum at the peak. Two components with different line widths exist in the latter profile: a narrow component (NC) with a full width half maximum of about 50 km s^{-1}, and a broad component (BC) with a full width zero intensity of more than 200 km s^{-1}. Such coexistence of two components has been often observed in HeI 5876Å, CaII, and FeII lines of other T Tauri stars (e.g., Batalha et al. 1996, Muzerolle, Hartmann, & Calvet 1998, Beristain, Edwards, & Kwan 1998), and both the components are considered to be associated with mass accretion in the vicinity of the star (e.g., Najita et al. 2000, and references therein). As shown in Fig. 4, Hα profiles have a red absorption dip indicative of infalling material to the star. The Hα and HeI profiles observing in 1999 are characterized by a shallower redshifted absorption dip and a weaker broad component, respectively, and such relation between the Hα dip and the HeI broad component suggests that the latter component arises from gas accreting to the star. No prominent emission associated with the Hα wings was found in the broad component of HeI in 1999: thus, we conclude that the Hα wings have a different origin from that of the broad component of the HeI line.

4 Discussion

4.1 Origin of Hα emission

Positional displacement as measured by spectroastrometry should be sensitive to any asymmetric structure about the continuum source. In the case of Hα emission from pre-main-sequence stars, binary companions are responsible for the displacement as shown by Bailey (1998a). However, the feature seen in RU Lupi is quite unlike those normally seen in binary systems which are not symmetric about the line centre. Binary stars with the same spectrum and different radial velocities could produce the observed positional displacement, although such motion at the observed direction does not agree with the orbital motion perpendicular to the outflow. No binary companion has been detected by *the Hubble Space Telescope* (Bernacca et al. 1995) or infrared speckle observations (Ghez et al. 1997). Thus, it is likely that the detected feature reflects the distribution of circumstellar matter around the star.

A variety of mechanisms have been previously proposed to explain the observed Hα profiles from pre-main-sequence stars. Magnetically-driven stellar winds which accelerate with distance have been suggested for Balmer emission including Hα (e.g., Decampli 1981; Hartmann, Edwards, & Avrett 1982; Lago 1984; Natta, Giovanardi, & Palla 1988), while a decelerating "stochastic" stellar wind was proposed by Mitskevich, Natta, & Grinin (1993). Calvet & Hartmann (1992) and Hartmann, Hewett & Calvet (1994) argue that the Hα emission is produced in infalling envelopes. Edwards et al. (1994) presented for 15 T Tauri stars a set of high resolution profiles including Balmer, HeI, and NaI lines and showed that the blue/red asymmetry of upper Balmer lines agrees well with magnetospheric accretion models. On the other hand, Reipurth, Pedrosa, and Lago (1996) compared their Hα profiles with various models, and suggested that a single model cannot account for the variety of the Hα profiles. In addition to outflowing and inflowing motion, Keplerian rotation would also be responsible for the shape of the Hα profile.

Among these candidates, we consider bipolar outflow as a plausible explanation for the observed displacement for the following reasons: (1) the positional displacement of the blue-shifted component is in the same direction as those of forbidden lines, which are considered to trace outflow, and (2) the other permitted lines, which probe mass accretion, do not have such broad wings as Hα, thus these wings should have different origin (cf. §3-3). No clear evidence for inflowing motion has been detected in the position spectra, consistent with previous models which propose that the Hα emission arises from a region within less than ten stellar radii (e.g., Calvet & Hartmann 1992; Hartmann, Hewett & Calvet 1994). Rotation cannot explain the observed displacement for the following reasons:

(1) the measured velocity increases with positional displacement while Keplerian rotation should behave in an opposite fashion, and (2) the star needs to be more than 100 $M_\odot$ to bound the gas with the measured positional displacement and velocity (3 au and 200 km s^{-1}, respectively) while previous research suggests the mass of the star is 0.5-2 $M_\odot$ (Gahm et al. 1974; Lamzin et al. 1996).

Figs 2 and 3 show that the velocity of the outflowing gas increases with positional displacement, a tendency which agrees with that of magnetically-driven wind models which predict that the flow accelerates with distance (e.g., Decampli 1981; Hartmann, Edwards, & Avrett 1982; Lago 1984). Most of the models adopt a spherically symmetric line forming region not exceeding ten stellar radii, and predict that the acceleration of the flow ends within this scale. On the other hand, the observed position spectra of RU Lupi indicate bipolar geometry and a velocity gradient extending to a few au (Figs 2 and 3). The latter results would indicate slower acceleration of the outflow than those predicted by models, however, models with more appropriate geometry and direct prediction of the positional displacement are necessary for detailed comparison. Actually, Hα emission from pre-main-sequence stars should be optically thick (cf. Reipurth, Pedrosa, & Lago 1996), thus the observed velocity field would be highly sensitive to the geometry which affects radiative transfer.

The time variation of the positional displacement and the intensity profile for the Hα wings are similar to that of HeI in the following points: there is no clear difference between 1996 and 1997, and a remarkable difference between 1997 and 1999. Since the HeI emission is related to the accreting gas, as shown in §3-3, such similar time variation suggests that the accreting gas also contributes to the Hα flux at least in 1996 and 1997. Even if the positional displacement of the bipolar outflow is constant over time, the net positional displacement can change as the flux of the accreting gas at the centre varies. Transient time variation of the displacement in high-velocity wings could be explained by direct motion of the outflowing ionized gas, although we reject this possibility since line profiles with the same velocities only show slight change of line-to-continuum ratio at the same velocities.

Here we attempt to explain the observed positional displacement with a steady bipolar outflow and time-variable flux from inflow. To remove contamination from inflow on the total Hα flux, and reproduce the position spectra of the outflow we make the the following assumptions: (1) the Hα emission from infalling gas arises from the star and cannot be spatially resolved by our observations, (2) inflow contributes to the observed Hα profiles only in 1996 and 1997, and (3) the time variation of the Li equivalent widths shown in Table 1 is due to the veiling continuum. The first assumption provides the observed net positional displacement as follows:

$$\Delta x_\lambda = \Delta x_{\lambda \mathrm{out}} \cdot \frac{I_{\lambda(\mathrm{out})}}{I_{\lambda(\mathrm{out})} + I_{\lambda(\mathrm{in})}} \qquad (1)$$

where Δx_λ is the net displacement shown in Fig. 4, $\Delta x_{\lambda \mathrm{out}}$ is the positional displacement caused by the bipolar outflow, $I_{\lambda(\mathrm{out})}$ and $I_{\lambda(\mathrm{in})}$, are the absolute Hα intensity from the outflow and inflow, respectively. This assumption is consistent with our observations, and the previous inflow models described above. From the second assumption, the intensities from the outflow and inflow are obtained as follows:

$$I_{\lambda(\mathrm{out})} = I_{\lambda(\mathrm{H}\alpha 99)}, \qquad I_{\lambda(\mathrm{in})} = I_{\lambda(\mathrm{H}\alpha)} - I_{\lambda(\mathrm{H}\alpha 99)}, \qquad (2)$$

where $I_{\lambda(\mathrm{H}\alpha)}$ is the absolute Hα intensity in a certain observing run, and $I_{\lambda(\mathrm{H}\alpha 99)}$ is that observed in 1999. This assumption is plausible for the Hα wings since those observed in 1999 are not associated with the other permitted lines indicative of mass accretion as described in 3-3. The third assumption provides the absolute Hα intensities from the observed parameters as follows:

$$\frac{I_{\lambda(\mathrm{H}\alpha)}}{I_{\lambda(\mathrm{H}\alpha 99)}} = \frac{i_{\lambda(\mathrm{H}\alpha)} \cdot I_{\lambda(\mathrm{conn})}}{i_{\lambda(\mathrm{H}\alpha 99)} \cdot I_{\lambda(\mathrm{conn99})}} = \frac{i_{\lambda(\mathrm{H}\alpha)}}{i_{\lambda(\mathrm{H}\alpha)}} \cdot \frac{W_{\lambda(\mathrm{Li99})}}{W_{\lambda(\mathrm{Li})}}, \qquad (3)$$

where $i_{\lambda(\mathrm{H}\alpha)}$ and $I_{\lambda(\mathrm{conn})}$ are the relative Hα intensity to the continuum and the absolute intensity of the continuum in a certain observing run, respectively, and $i_{\lambda(\mathrm{H}\alpha 99)}$ and $I_{\lambda(\mathrm{conn99})}$ are those observed in 1999. $W_{\lambda(\mathrm{Li})}$ and $W_{\lambda(\mathrm{Li99})}$ are the equivalent widths of the Li absorption in a certain observing run and in 1999, respectively. By combining equations (1)-(3), the positional displacement of the outflow is obtained from the observed parameters as follows:

$$\Delta x_{\lambda(\mathrm{out})} = \Delta x_{\lambda} \cdot \frac{i_{\lambda(\mathrm{H}\alpha)}}{i_{\lambda(\mathrm{H}\alpha 99)}} \cdot \frac{W_{\lambda(\mathrm{Li99})}}{W_{\lambda(\mathrm{Li})}}, \qquad (4)$$

Fig. 6 shows the reproduced position spectra using equation (4). The spectra for 1999 are identical with the observed one shown in Fig. 4, since we assume that the outflow dominates the observed intensity in this observing run. These spectra agree well with each other, thus support the idea that the time variation of the positional displacement can be explained by the combination of steady bipolar outflow and time-variable flux from the accreting gas.

The contribution of the inflow to the total Hα flux could be estimated from equations (2) and (3): according to these equations, 32 and 28 percents of the total Hα flux would arise from the accreting gas in 1996 and 1997, respectively. These values would be lower limits, since the inflow with low velocities would contribute to the Hα emission in 1999. The permitted lines related to mass accretion were detected with a typical velocity range between -150 and $+150$ km s^{-1} as shown in §3-3, and there is no reason to assume that Hα emission does not arises from the same region.

4.2 Origin of the forbidden lines

Optical forbidden emission lines including [OI] 6300Å and [SII] 6716/6731Å provide information on the outflows from T Tauri stars. These line profiles often have two blue-shifted velocity components: a high-velocity component (HVC) and low-velocity component (LVC) which have typical velocities of -50 to -150 km s^{-1} and -5 to -20 km s^{-1}, respectively (Hirth, Mundt, and Solf 1997). The HVC is spatially resolved by ground-based long-slit spectroscopy in the nearest star-forming regions (e.g., Solf & Böhm 1993; Hirth, Mundt, and Solf 1997). Hirth, Mundt, and Solf (1997) have shown that the typical angular scale of the HVC is 0.2–0.6 arcsec from their large sample of data mainly in the Taurus-Auriga cloud. The high speed and narrow linewidth of the HVC indicates that the velocity vectors of the contributing gas particles are nearly parallel to one another, i.e., suggesting a well-collimated flow or jet (Kwan & Tademaru 1988). On the other hand, the low-velocity component (LVC) has smaller angular scales in the same sample (0.1-0.2 arcsec or less), and its origin is less understood. Geometric effects of a single outflow are proposed to explain the existence of the two velocity components (e.g., Edwards et al. 1987; Hartmann & Raymond 1989), while two distinct mechanisms, jet and disc wind, are proposed for each velocity component by Kwan and Tademaru (1988, 1995). Hamann (1994) measured the electron density, temperature, and the ionization state between the HVC and LVC in many T Tauri stars, and the measured difference of the physical conditions suggest distinct origins for these two components as proposed by Kwan and Tademaru (1988, 1995). Similar results were also presented by Hartigan, Edwards, & Ghandour (1995). The velocity dispersion and flow velocity are comparable in the LVC, suggesting moderate collimation such as that due to a disc wind (e.g., Solf & Böhm 1993). Most pre-main-sequence stars do not have red-shifted components to their forbidden lines, and this is explained by obscuration of these components by circumstellar discs (e.g., Eislöffel et al. 2000, and references therein).

The [OI] and [SII] lines from RU Lupi have two blue-shifted components, and our results also support the existence of two distinct mechanisms. The [SII] intensity ratio indicates different electron densities between the HVC and LVC as shown in §3-2 (4-6$\times 10^3$ and more than 10^4-10^5 cm^{-3} assuming a electron temperature of 10^4 K), a tendency also observed in other T Tauri stars by Hamann (1994). In addition, the intensity of each component exhibits different time variations as described in §3-2. The coexistence of two distinct mechanisms can easily explain these differences.

Furthermore, the velocity field in the LVC shown in Fig. 3 agrees with the disc wind hypothesis. Fig. 3 shows that the position of the LVC is offset from the star even at zero velocity and nearly constant over all velocities in [OI] emission, as described in §3-2. The former cannot be explained by acceleration of outflow, while both tendencies can easily be explained by moderate collimation and/or rotation which would be expected in a disc wind. In the case of [SII] 6731Å, the positional displacement in the LVC increases with the velocity. Such discrepancy between the [OI] and [SII] emission can be explained by blending of the HVC and LVC near their boundary. The profiles of the forbidden lines in Fig. 2 show that the two components are partially blended, thus contamination from the HVC could increase the positional displacement in the LVC near their boundary. It is likely that this effect is more prominent for the [SII] line, since the lower critical density of this line allows for larger contamination from the HVC which has a lower electron density (cf. §3-2).

4.3 Circumstellar disc and disc gap

As shown in Fig. 2, the forbidden lines have only blue-shifted components, similar to many other T Tauri stars, a fact usually explained by obscuration of the red-shifted flow by a circumstellar disc (e.g., Eislöffel et al. 2000, and references therein). Infrared excess and a bright millimetre continuum suggest the existence of a circumstellar disc around RU Lupi (e.g., Giovannelli et al. 1995; Carballo et al. 1992; Nürnberger et al. 1997), supporting the explanation for the lack of red-shifted components.

On the other hand, Hα emission has both blue- and red-shifted components. The measured positional displacement for the Hα emission is smaller than any velocity component of [OI] and [SII] emission. The detection of the red-shifted Hα outflow can be explained by a gap in the disc which allows this emission to be seen. The presence of disc holes and gaps is often inferred around other pre-main-sequence stars by infrared spectral energy distributions (SEDs) (e.g., Mathieu et al. 1991; Marsh & Mahoney 1992; Jensen & Mathieu 1997), and directly observed in near-infrared imaging (e.g., Roddier et al. 1996; Silber et al. 2000) and at radio wavelengths (e.g., Dutrey, Guilloteau, & Simon 1994). Fig. 3 suggests that the projected radius of the hole or gap is 20-30 milliarcsec, which corresponds to 3-4 au, assuming symmetric distribution of the blue-shifted and unseen red-shifted components of the forbidden lines.

To investigate the presence of a disc gap, we plot the infrared SED in Fig. 7. The flux at $JHKLM$-bands and 12, 25, 60, 100 μm were obtained from Giovannelli et al. (1995) and Carballo et al. (1992). Giovannelli et al. (1995) show the near-infrared flux is highly variable with time, thus the data-set with the largest and smallest flux were selected from their data and plotted in the figure. In Fig. 7, a spectrum obtained via the *Infrared Space Observatory* (ISO) data archive is also plotted to interpolate the flux in the mid-infrared. Lamzin et al. (1996) claim that the mid-to-far infrared flux obtained by Carballo et al. (1992) would be overestimated, since another source discovered by Cohen & Schwartz (1987) is included in the same aperture. However, the consistency of their data with the ISO spectrum shows that the contribution from this source is much less than the total flux: the aperture of the ISO Short-Wave Spectrometer (SWS) with a size of 20×33 arcsec^2 does not include this source which lies about 3 arcmin away from the target.

Fig. 7 shows two peaks in the SED which arises from dust. The near-infrared peak at 1.65 μm is longer than the peak for the star (1.0 μm) with an effective temperature of 3900 K (Nürnberger et al. 1997; Lamzin et al. 1996). Previous authors show that the selective extinction towards RU Lupi is 0.3-1.3 A$_V$ (Hughs et al. 1994; Giovannelli et al. 1995). Such values can shift the peak of the stellar continuum by less than 0.2 μm suggesting that the near-infrared excess from the stellar photosphere represents hot dust from the accretion disk. Such a contribution by the accretion disk to the near-infrared SED is also supported by the near-infrared colours (J-H and H-K of 0.84-0.92 and 0.72-0.77, respectively) and diagrams shown by Hughes et al. (1994), Greene & Meyer (1995), and Itoh et al. (1999). On the other hand, the mid-to-far infrared SED shows another excess which is due to cooler dust with a temperature of less than 100 K. The shallow dip at 4-15 μm suggests a lack of dusty material at temperatures of 200-900 K. These temperatures correspond to the radiative temperature at a radius of 0.1-2 au from the star, assuming the total luminosity from the star and accreting gas of 5 $L_\odot$ based on Lamzin et al. (1996). These spatial scales agree well with that of the suggested gap in Figs 2 and 3.

Theoretical work has shown that disc gaps and holes could be induced by binary companions or young planets (e.g., Lubow & Artimowicz 2000). In the case of RU Lupi, no other pre-main-sequence companions have been detected by *Hubble Space Telescope* (Bernacca et al. 1995), infrared speckle observations (Ghez et al. 1997), or spectro-astrometry which is sensitive to the presence of binaries (cf. Bailey 1998a). Therefore, the observed disc gap suggests the existence of an unseen companion. A young planet could be one of possible candidates for the following reasons: the presence of the fragmented dusty clouds around RU Lupi are suggested by variability at optical to infrared wavelengths (Gahm et al. 1974; Giovannelli et al.1995), and Gahm et al. (1974) claim that such clouds would indicate ongoing planetary formation around this object. In addition, the observed disc gap has a similar size to that of the orbit of the Jovian planets in our solar system, and Takeuchi, Miyama, & Lin (1996) suggest that a proto-Jupiter could induce a disc gap with a similar size to its orbit. Their numerical calculations show that a Saturnian and Jovian mass protoplanet can open a gap in 10^3-10^4 and 10^2-10^3 yrs, respectively, timescales which are much shorter than the age of RU Lupi (10^6 yrs - Lamzin et al. 1996).

5 Conclusions

Spectro-astrometric observations have been used to determine the spatial distribution of optical emission lines from RU Lupi. Positional displacements were detected in Hα, [OI] 6300 Å, [SII] 6731/6716 Å, and [NII] 6583 Å with accuracies down to a few milli-arcsec. The intensity profiles were also obtained for these lines together with HeI, FeI, FeII, SiII, and another [OI] line.

The positional displacement of Hα emission extends towards the south-west and north-east with angular scales of 20-30 milli-arcsecs. The blue-shifted wing in the intensity profile corresponds to the displacement at the south-west while the red-shifted wing corresponds to that at the north-east. We conclude that the positional displacement of the Hα emission is due to bipolar outflow for the following reasons: (1) the distribution of the positional displacement is almost symmetric between the blue-shifted and red-shifted components, (2) the displacement of the blue wing aligns well with that of the forbidden lines which are considered to trace outflowing gas. The velocity of the outflow increases with the distance, suggesting the flow is magnetically-driven. On the other hand, the time variation of the intensity profile and the positional displacement can be explained well by the variation of Hα flux from the accreting gas at the star. We estimate the contribution of the accreting gas to the total flux to be more than 32 and 28 percent in 1996 and 1997, respectively.

The positional displacement of [OI] and [SII] emission extends towards the south-west, in the same direction as HH55 which lies 3' from the star. The intensity profiles have two blue-shifted components, as seen in many other pre-main-sequence stars, and the positional displacements of hundreds of milli-arcsecs and down to 30 milli-arcsecs were detected for the high-velocity components (HVC) and the low-velocity components (LVC), respectively. The differences of the derived electron density and time variation between the two components suggest that these components have distinct origins, e.g., jet and disc wind. The positional displacement in the LVC is consistent with the LVC originating from a disc wind.

The forbidden lines have only blue-shifted components, as do those in many other T Tauri stars, and this is usually explained by the obscuration of the red-shifted flow by a circumstellar disc. On the other hand, the Hα outflow has both blue-shifted and red-shifted components. Such a difference suggests the presence of a disc gap with an outer radius of 3-4 au. The infrared spectral energy distribution is consistent with the presence of a gap on this scale. This gap could be induced by a unseen companion such as a young planet.

We would like to thank the staff at the Anglo-Australian Observatory for their help and support during the observations. We also thank ISO staff for their assistance in using their archive system, and the referee (T.P. Ray) for his valuable comments. MT thanks PPARC for support through a PDRA.

References

Bailey J., 1998a, MNRAS, 301, 161

Bailey J., 1998b, SPIE Proceeing, 3355, 932

Batalha C.C., Stout-Batalha N.M., Basri G., Terra M.A.O., 1996, ApJS, 103, 211

Beristain G., Edwards S., Kwan J., 1998, ApJ, 499, 828

Bernacca P.L., Lattanzi M.G., Porro, I., Neuhäuser R., Bucciarelli B., 1995, A&A, 299, 933

Burrows C.J., Stapelfeldt K.R., Watson A.M., Krist J.E., Ballester G.E., Clarke J.T., Crisp D., Gallagher J.S.III, Griffiths R.E., Hester J.J., Hoessel J.G., Holtzman J.A., Mould J.R., Scowen P.A., Trauger J.T., Westphal J.A. 1996, ApJ, 473, 437Calvet N., Hartmann L., 1992, ApJ, 386, 239

Calvet N.,Hartmann L., Hewett R., 1992, ApJ, 386, 229

Carballo R., Wesselius P.R., Whittet D.C.B., 1992, A&A, 262, 106

Cohen M., Schwartz R.D., 1987, ApJ, 316, 311

Decampli W.M., 1981, ApJ, 244, 124

Devaney M.N., Thiébaut E., Foy R., Blazit A., Bonneau D., Bouvier J., de Batz B., Thom Ch., 1995, A&A, 300, 181

Dutrey A., Guilloteau S., Simon M., 1994, A&A, 286, 149

Edwards S., Cabrit S., Strom S.E., Heyer I., Strom K.M., Anderson E., 1987, ApJ, 321, 473

Edwards S., Hartigan P., Ghandour L., Andruis C., 1994, AJ, 108, 1056

Eislöffel J., Mundt R., Ray T.P., Rodríguez L.F, 2000, Protostars and Planets IV, 815

Gahm G.F., Nordth H.L., Olofsson S.G., Carlborg N.C.J., 1974, A&A, 33, 399

Gahm G.F., Lago M.T.V.T., and Penston M.V., 1981, MNRAS, 195, 59

Ghez, A.M. McCarthy D.W., Patience J.L., Beck T.L., 1997, ApJ, 481, 378

Giovannelli F., Vittone A.A., Rossi C., Errico L., Bisnovatyi-Kogan G.S., Kurt V.G., Lamzin S.A., Larionov M., Sheffer E.K., Sidorenkov V.N. 1995, 114, 341Greene T.P., Meyer M.R., 1995, ApJ, 450, 233

Hamann F., 1994, ApJS, 93, 485

Hamann F. Persson S.E., 1992, ApJS, 82, 247

Hartigan P., Edwards S., Ghandour L., 1995, ApJ, 452, 736

Hartmann L., Hewett R., Calvet N., 1994, ApJ, 426, 669

Hartmann L., Edwards S., Avrett E., 1982, ApJ, 261, 279

Hartmann L. Raymond J.C., 1989, ApJ, 337, 903

Hirth G.A., Mundt R., Solf J., 1994, A&A, 285, 929

Hirth G.A., Mundt R., Solf J., 1997, A&AS, 126, 437

Hughes J., Hartigan P., Clampitt L., 1993, AJ, 105, 571

Hughes J., Hartigan P., Krautter J., Kelemen J., 1994, AJ, 108, 1071

Itoh Y., Tamura M., Nakajima T., 1999, AJ, 117, 1471

Jensen E.L.N. Mathieu R.D., 1997, AJ, 114, 301

Krautter J., Reipurth B., Eichendorf W., 1984, A&A, 133, 169

Kwan J. Tademaru E., 1988, ApJ, 332, L41

Kwan J. Tademaru E., 1995, ApJ, 454, 382

Lamzin S.A., Bisnovatyi-Kogan G.S., Errico L., Giovannelli F., Katysheva N.A., Rossi C., Vittone A.A. 1996, A&A, 306, 877Lago M.T.V.T, 1984, MNRAS, 210, 323

Lago M.T.V.T, Penston M.V., 1982, MNRAS, 198, 429

Lubow S., Artimowicz P., 2000, Protostars and Planets IV, 731

Marsh K.A. Mahoney M.J., 1992, ApJ, 395, L115

Mathieu R.D., Adams F.C., Latham D.W., 1991, AJ, 101, 2184

Mitskevich A.S., Natta A., Grinin V.P., 1993, ApJ, 404,751

Muzerolle J., Hartmann L., Calvet N., 1998, AJ, 116, 455

Najita J., Edwards S., Barsi G., and Carr J., 2000, Protostars and Planets IV, 457 Natta A., Giovanardi C., Palla F., 1988, ApJ, 332, 921

Nürnberger D., Chini R., and Zinnecker H., 1997, A&A, 324, 1036

Osterbrock D.E., 1989, Astrophysics of Gaseous Nebulae and Active Galactic Nuclei (Mill Valley: Univ. Science Books)

Osterbrock D.E., Tran H.D., Veilleux S., 1992, ApJ, 389, 305

Ray T.P., Mundt R., Dyson J.E., Falle S.A.E.G., Raga A.C., 1996, ApJ, 468, L103

Reipurth B., Pedrosa A., Lago M.T.V.T., 1996, A&AS, 120, 229

Roddier C., Roddier F., Northcott M.J., Graves J.E., Jim K. 1996, ApJ, 463, 326

Silber J.M., Gledhill T.M., Duchêne G., Ménard F. 2000, ApJL, 536, 89

Solf J., Böhm K.H., 1993, ApJ, 410, L31

Takeuchi T., Miyama S.M., Lin D.N.C., 1996, ApJ, 460, 832

Table 1: The equivalent widths of the emission lines.

Wavelength[a] (Å)	Line	Equivalent Width (Å)[b]		
		25-Aug-96	27-Jun-97	2-Jul-99
6191.56	FeI	-	-	0.057
6238.38	FeII	-	-	0.28
6247.56	FeII	-	-	0.61
6300.23	[OI]	-	-	1.70
6347.09	SiII	-	-	0.23
6363.88	[OI]	-	-	0.43
6371.36	SiII	-	-	0.31
6416.91	FeII	-	-	0.27
6432.65	FeII	-	-	0.73
6456.38	FeII	-	-	1.09
6517.02	FeII	-	-	1.08
6562.82	Hα	145	137	122
6678.15	HeI	2.24	2.09	1.23
6583.41	[NII]	-[c]	-[c]	-[c]
6707.82	Li	-0.16[d]	-0.20[d]	-0.27[d]
6716.47	[SII]	0.25	0.25	0.31
6730.85	[SII]	0.50	0.57	0.73

[a] References – Lago & Penston (1982), Osterbrock, Tran, & Veilleux (1992)

[b] Uncertainty of the measurement is 0.1 Å for Hα, and 0.03-0.05 Å for the others.

[c] The equivalent width was not measured because of the difficulty of the removal of the strong Hα wing.

[d] The equivalent widths of the absorption are displayed.

Table 2: [SII] equivalent widths & ratios

Line	Component	Equivalent Width (Å)		
		25 Aug 96	27 Jun 97	2 Jul 99
[SII] 6716 Å	HVC	0.15	0.13	0.18
	LVC	0.10	0.12	0.14
[SII] 6731 Å	HVC	0.25	0.24	0.34
	LVC	0.25	0.31	0.38
6716/6731	HVC	0.60	0.54	0.53
ratio	LVC	0.40	0.39	0.37

Note: the dividing velocity for the high velocity component (HVC) and low velocity component (LVC) is defined as -95 km s^{-1} in the stellar rest frame, as that defined by Hamann (1994). Uncertainty of the measured equivalent widths is about 0.02 Å.

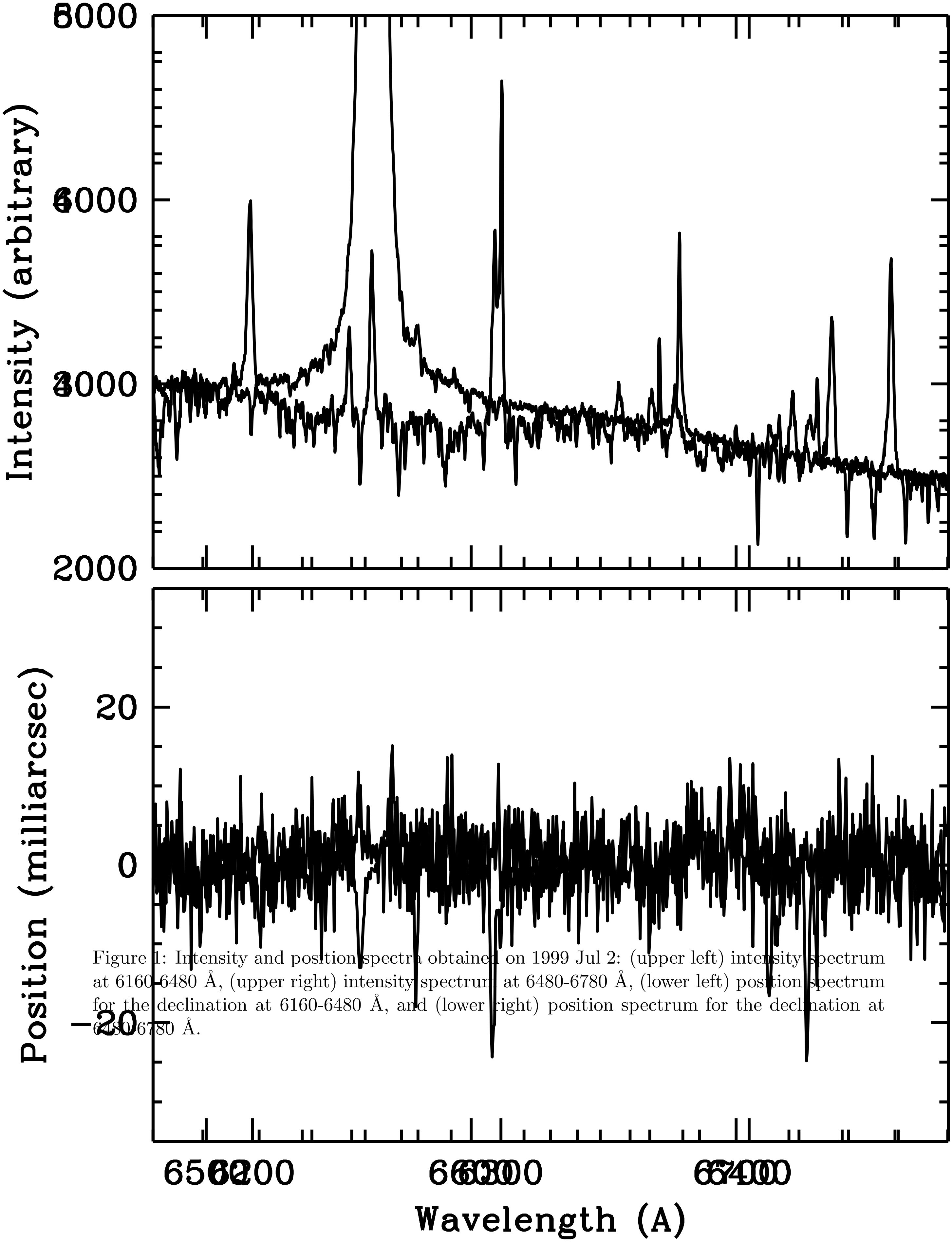

Figure 1: Intensity and position spectra obtained on 1999 Jul 2: (upper left) intensity spectrum at 6160-6480 Å, (upper right) intensity spectrum at 6480-6780 Å, (lower left) position spectrum for the declination at 6160-6480 Å, and (lower right) position spectrum for the declination at 6480-6780 Å.

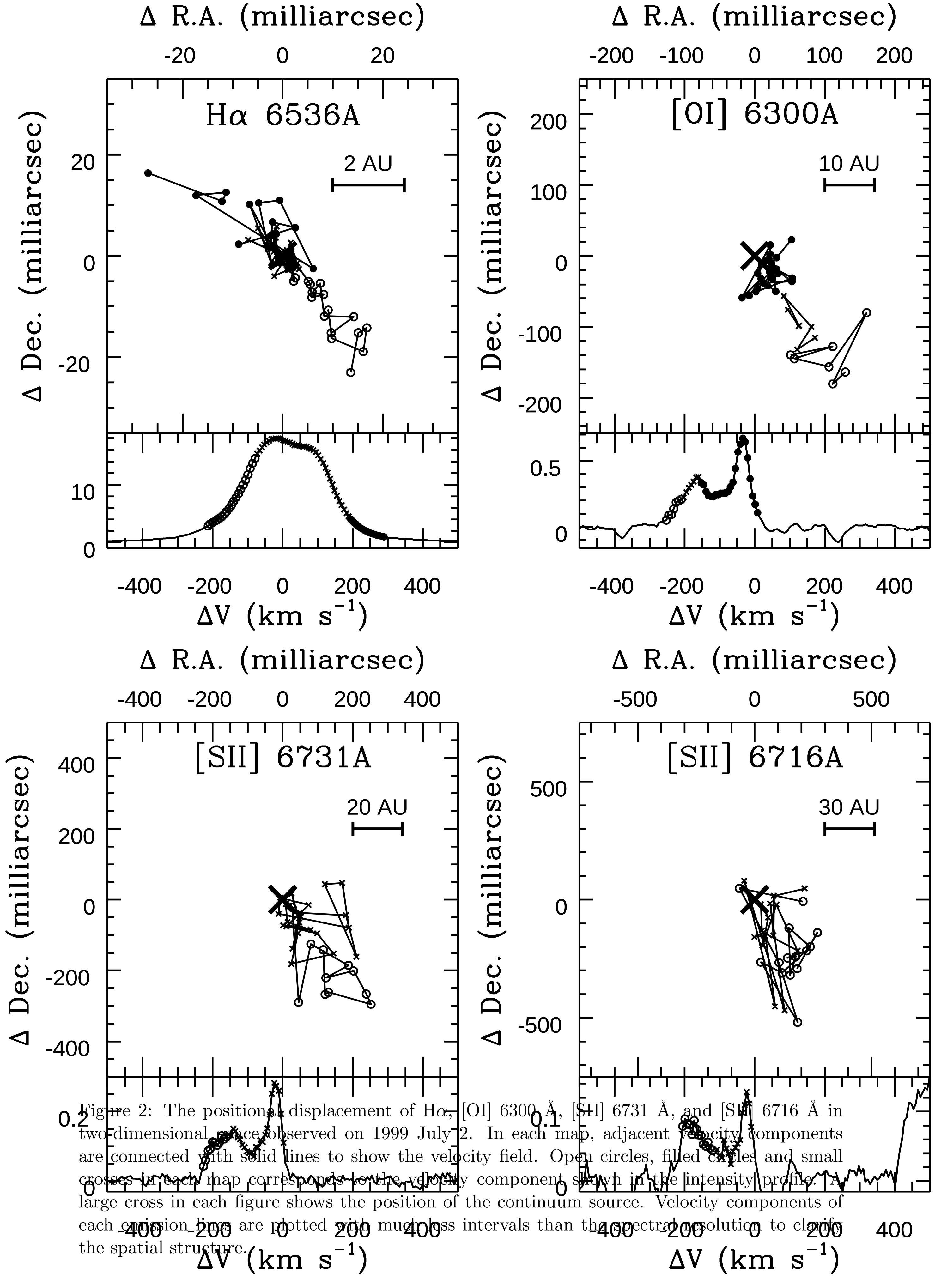

Figure 2: The positional displacement of Hα, [OI] 6300 Å, [SII] 6731 Å, and [SII] 6716 Å in two-dimensional space observed on 1999 July 2. In each map, adjacent velocity components are connected with solid lines to show the velocity field. Open circles, filled circles and small crosses in each map corresponds to the velocity component shown in the intensity profile. A large cross in each figure shows the position of the continuum source. Velocity components of each emission lines are plotted with much less intervals than the spectral resolution to clarify the spatial structure.

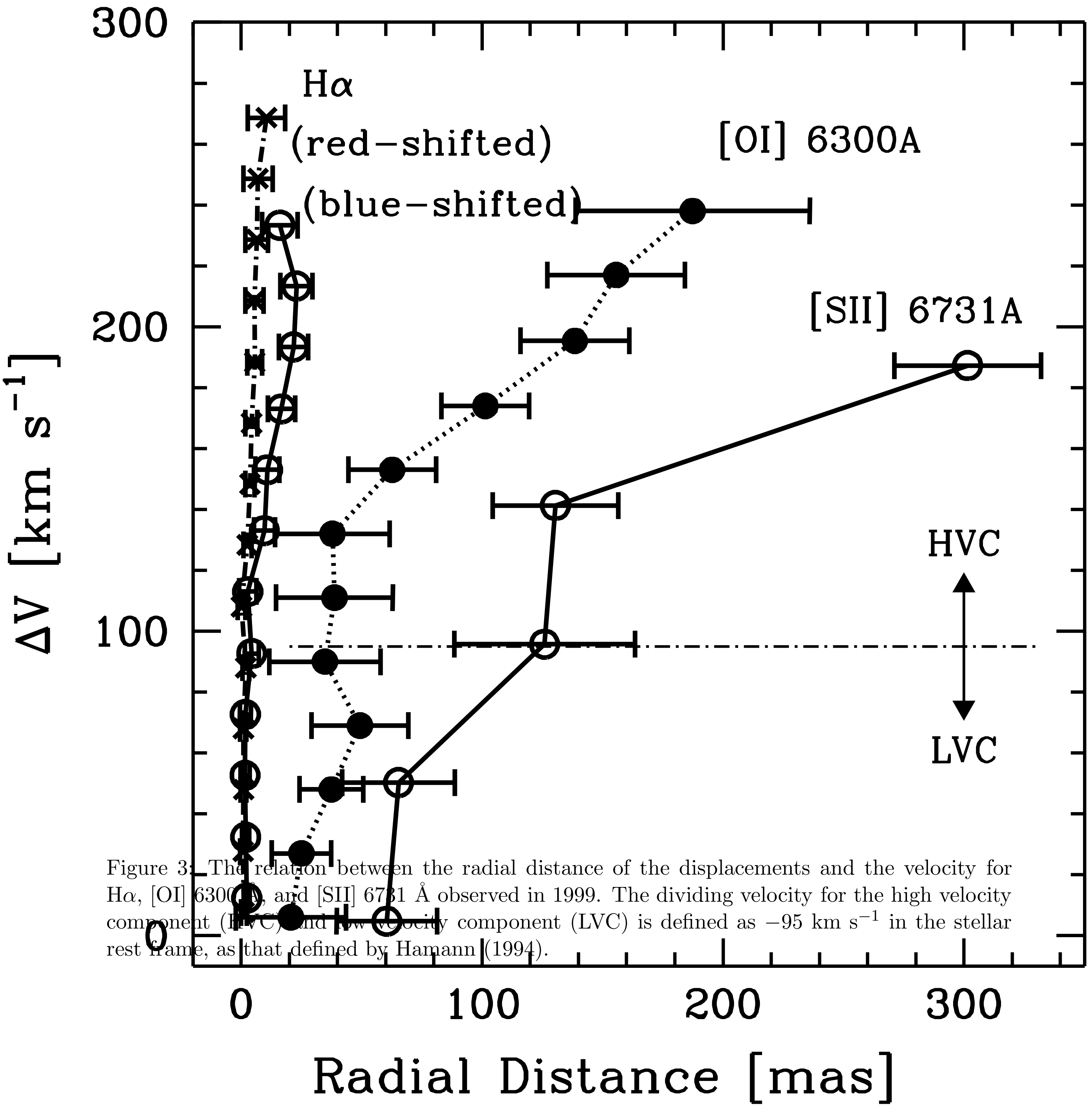

Figure 3: The relation between the radial distance of the displacements and the velocity for Hα, [OI] 6300 Å, and [SII] 6731 Å observed in 1999. The dividing velocity for the high velocity component (HVC) and low velocity component (LVC) is defined as -95 km s^{-1} in the stellar rest frame, as that defined by Hamann (1994).

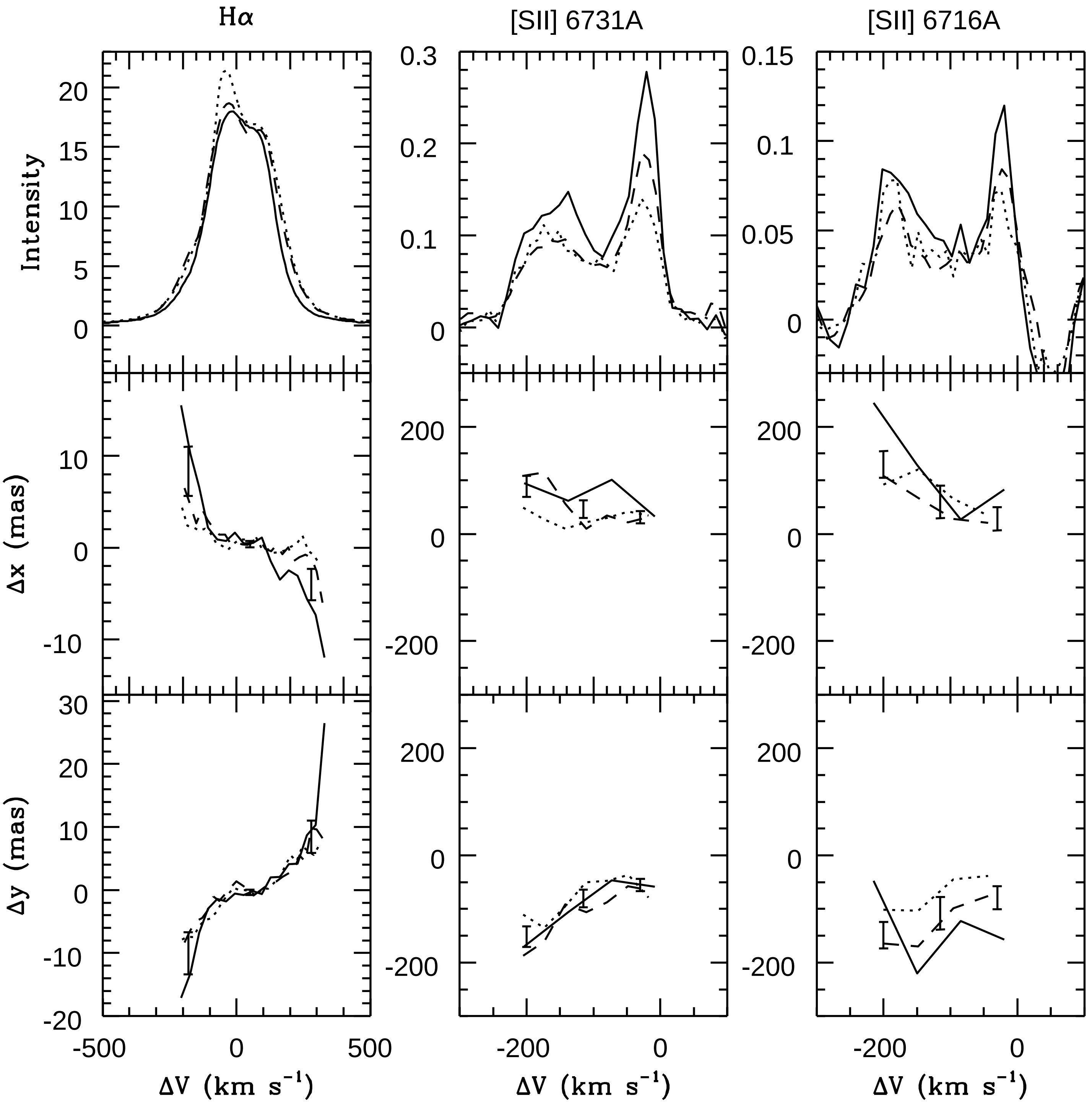

Figure 4: Time variation of the intensity and the positional displacement of Hα and [SII] 6731/6716Å emission. Dotted, dashed , and solid lines show the results observed in 1996, 1997, and 1999, respectively. The intensity of each line is normalized by that of the continuum. Vertical bars in the position spectra show typical uncertainties of the measurement.

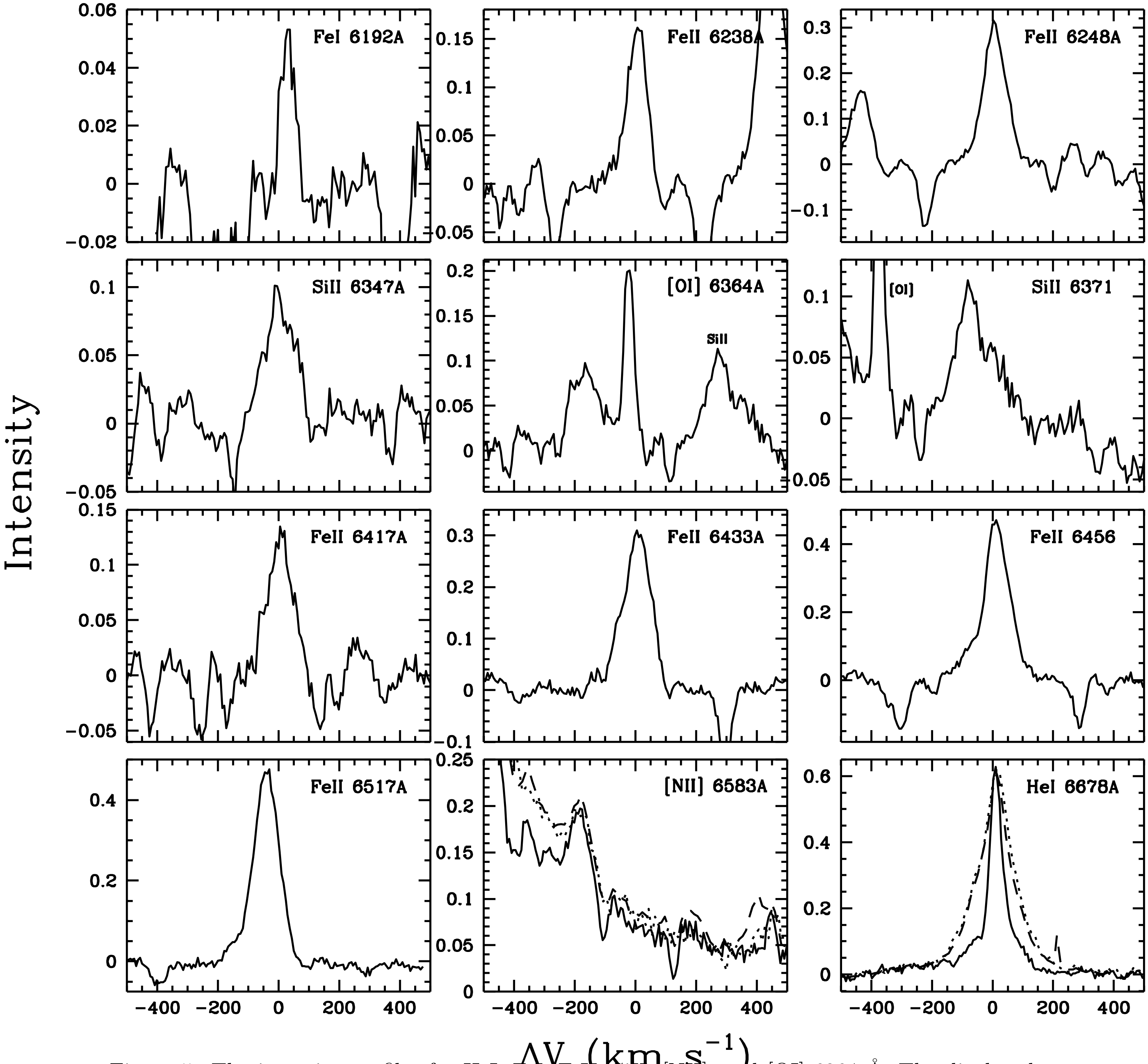

Figure 5: The intensity profiles for HeI, FeI, FeII, SiII, [NII], and [OI] 6364 Å. The displayed intensity in each figure is normalized by that of the continuum emission at the same wavelength. Solid curves in all the figures were observed in 1999, while dotted and dashed curves for [NII] and HeI were obtained in 1996 and 1997, respectively. The profiles of [NII] 6583 Å are contaminated by the strong Hα wing.

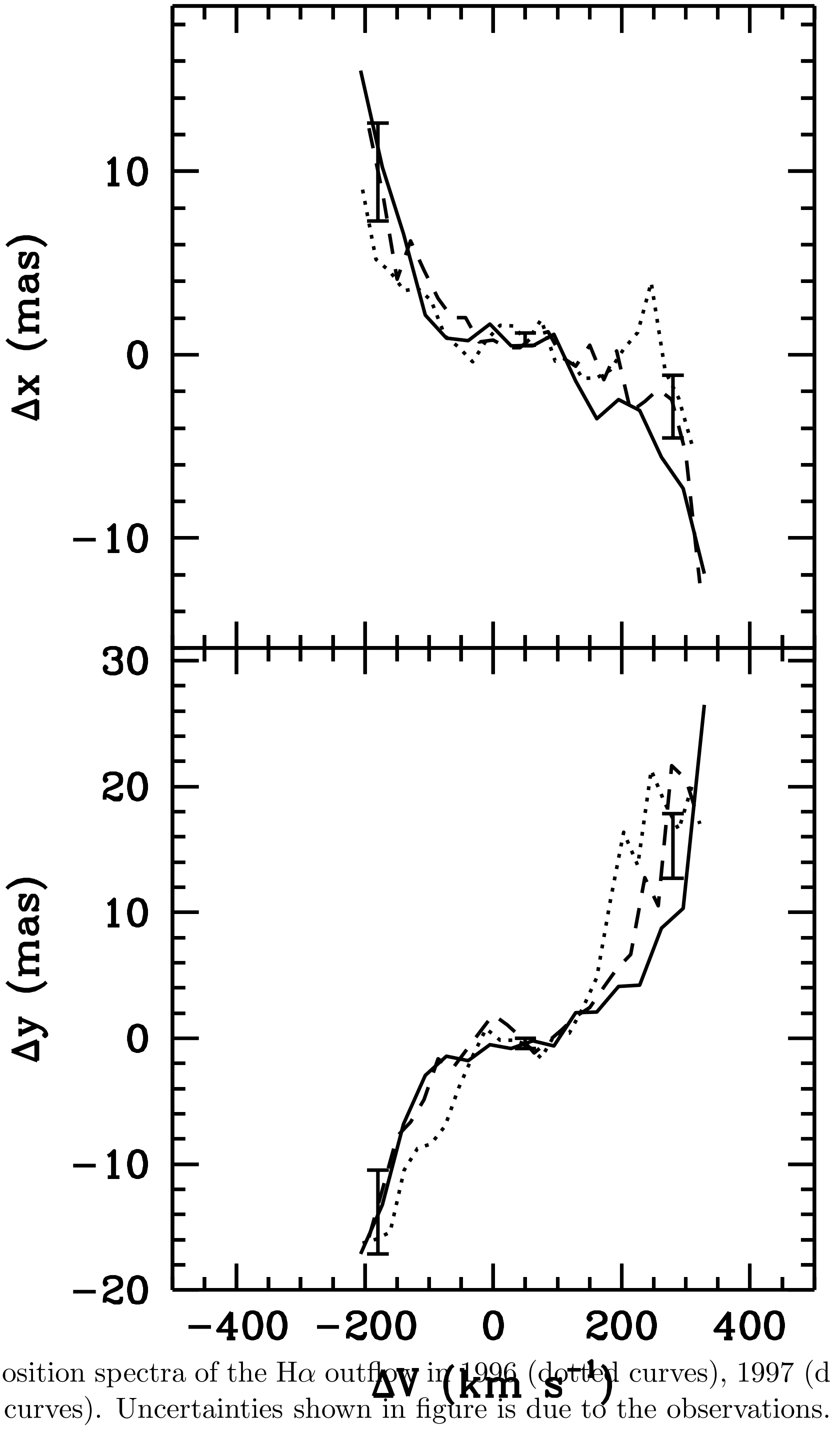

Figure 6: The position spectra of the Hα outflow in 1996 (dotted curves), 1997 (dashed curves), and 1999 (solid curves). Uncertainties shown in figure is due to the observations.

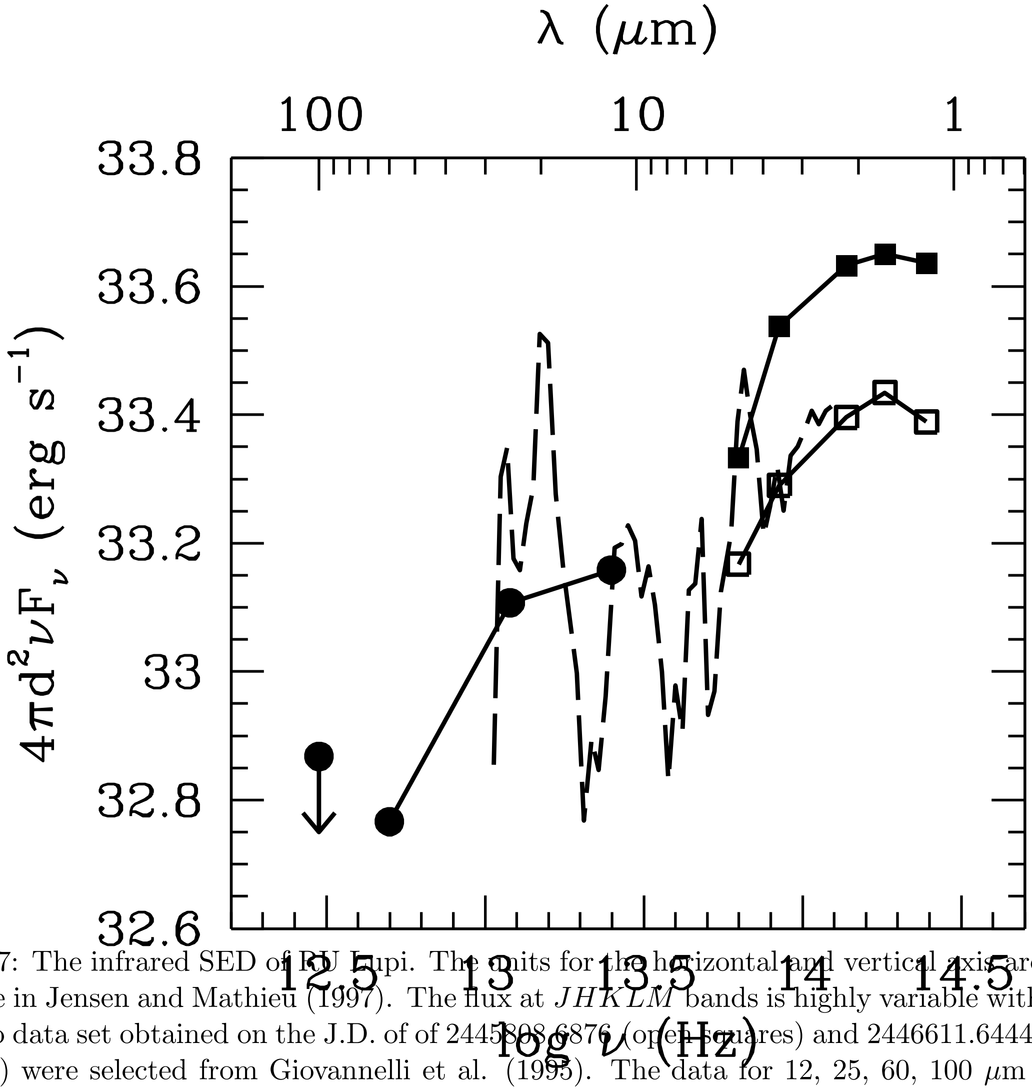

Figure 7: The infrared SED of RU Lupi. The units for the horizontal and vertical axis are same as those in Jensen and Mathieu (1997). The flux at *JHKLM* bands is highly variable with time, and two data set obtained on the J.D. of of 2445808.6876 (open squares) and 2446611.6444 (filled squares) were selected from Giovannelli et al. (1995). The data for 12, 25, 60, 100 μm shown with filled circles were obtained by *IRAS* observations. A mid-infrared spectrum obtained by ISO-SWS was smoothed along the wavelength to achieve higher signal-to-noise ratio, and plotted with a dashed line. The resultant spectral resolution ($\lambda/\delta\lambda$) of the spectrum is 20.